We are IntechOpen,
the world's leading publisher of
Open Access books
Built by scientists, for scientists

6,900
Open access books available

186,000
International authors and editors

200M
Downloads

154
Countries delivered to

Our authors are among the

TOP 1%
most cited scientists

12.2%
Contributors from top 500 universities

BOOK CITATION INDEX
CLARIVATE ANALYTICS
INDEXED

WEB OF SCIENCE™

Selection of our books indexed in the Book Citation Index
in Web of Science™ Core Collection (BKCI)

Interested in publishing with us?
Contact book.department@intechopen.com

Numbers displayed above are based on latest data collected.
For more information visit www.intechopen.com

Phosphor-Based White Light Emitting Diode (LED) for Vertical Scanning Interferometry (VSI)

Wee Keat Chong[1], Xiang Li[1] and Yeng Chai Soh[2]
[1]Singapore Institute of Manufacturing Technology, A*STAR
[2]Nanyang Technological University
Singapore

1. Introduction

Vertical scanning interferometry (VSI) is an established optical method for surface profile measurement by analyzing a series of interference patterns of low coherence light with known optical path difference among them. As white light is commonly used as low coherence light source, vertical scanning interferometry is also known as white light interferometry (WLI).

Vertical scanning interferometry is most commonly used as surface profilometer which is considered as an enabling and supporting technology to other fields such as surface finishing, machining and material science. It is a non-contact three-dimensional surface measurement technique that provides accuracy up to nanometer level and measurement range up to a few hundred micrometers.

Fig. 1 graphically illustrates the schematic diagram of vertical scanning interferometry in Michelson interferometer configuration; the light beam from the light source is split into two: one to reference surface and one to measurement surface, then these light beams reflect and interfere with each other. Interference pattern occurs when the optical path difference (OPD) between these two light beams is small, within the coherence length of the light source. The interference pattern is known as interferogram (as shown in Fig. 2), it is recorded by area-based photo-sensitive sensor such as CCD camera. Correlogram is the function of intensity response of each pixel against optical path difference, and it is further processed for height profile measurement. Fig. 3 graphically illustrates correlogram and coherence peak function of vertical scanning interferometry.

Apart from the light source, the hardware of vertical scanning interferometry has not changed much in the past one decade. As phosphor-based white light emitting diode (LED) promises greater power, longer lifetime, low heat dissipation and compactness, it is replacing the conventional light source in vertical scanning interferometry.

The conventional light source for white light has a very broad and smooth spectrum, for example Fig. 4 shows the spectrum of Quartz Tungsten Halogen Lamps (model no 6315 from NewPort). However due to the spectral response of photo detector, the effective spectrum of conventional white light is considered as single Gaussian function in visible light spectrum. On the other hand, phosphor-based white LED consists of single color LED
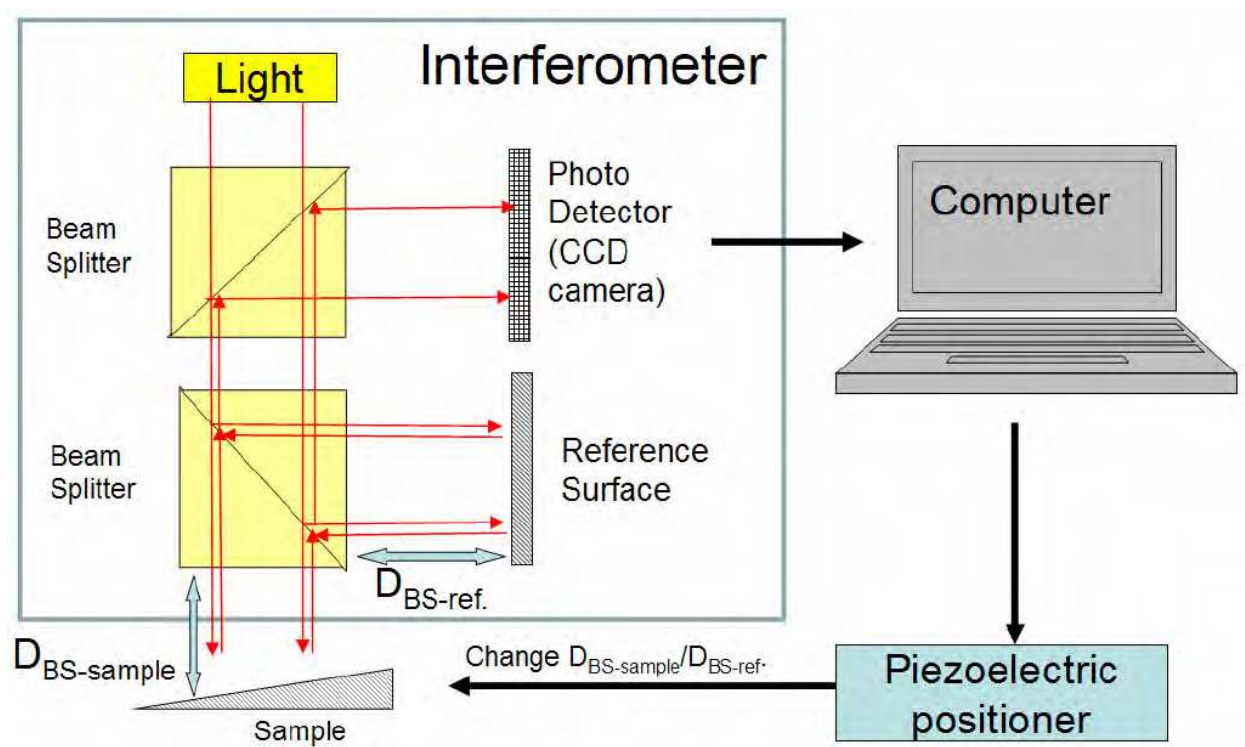
Fig. 1. Schematic diagram of vertical scanning interferometry in Michelson interferometer configuration.
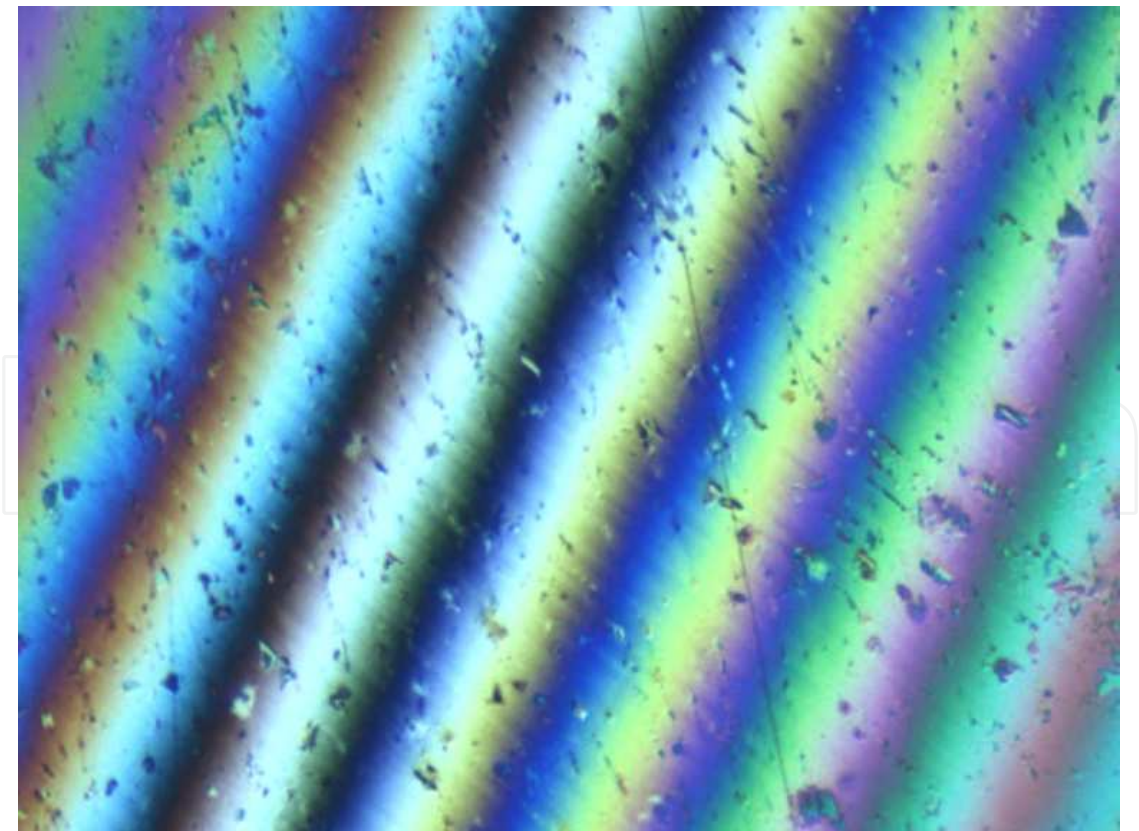

Fig. 2. Example of interferogram of vertical scanning interferometry: Fringe on a tilted flat surface captured using a CCD camera.
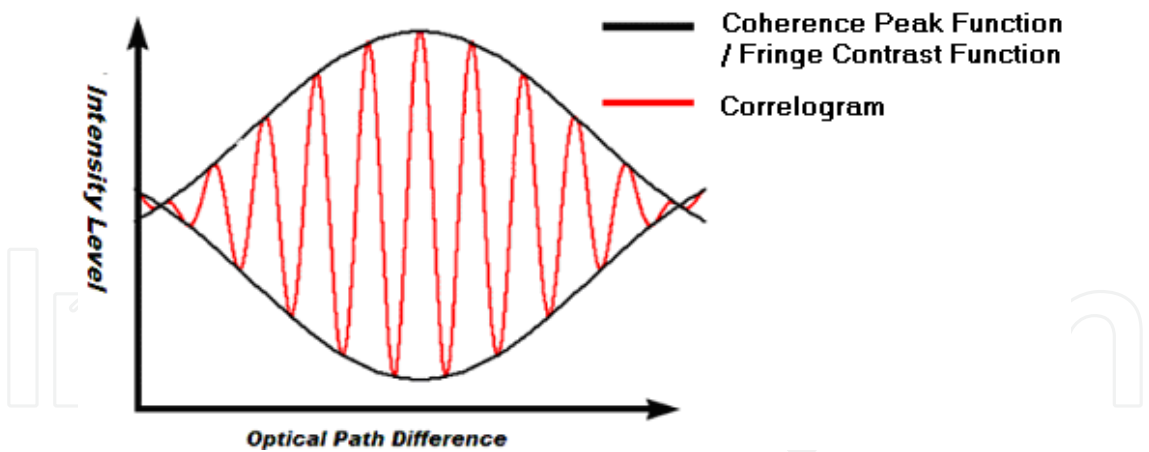
Fig. 3. Example of correlogram and corresponding fringe contrast function (also known as coherence peak function) in vertical scanning interferometry.

(normally blue) and phosphor of different color (normally yellow) to produce white light, so there are two peaks in its spectrum. Fig. 5 compares the effective intensity spectrum of conventional white light and phosphor-based white LED, the major difference between these two light sources is the number of peaks in spectral domain.
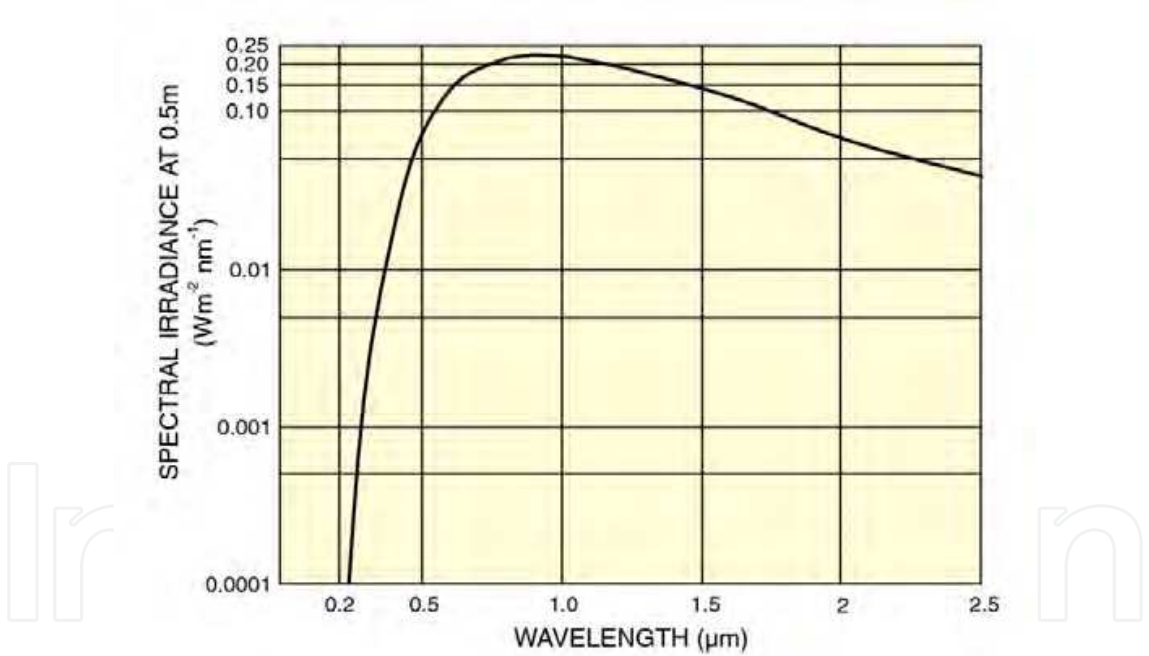

Fig. 4. Spectral irradiance at 0.5 m from the 6315 1000W QTH Lamp3 (by NewPort).

As most prior works (Guo, Zhao, & Chen, 2007; Gurov, Ermolaeva, & Zakharov, 2004; Mingzhou, Chenggen, Cho Jui, Ivan, & Shihua, 2005; Pavli?ek & Soubusta, 2004) assume the use of conventional white light, the effects of phosphor-based white LED on vertical scanning interferometer is the focus on this chapter. Other than that, this chapter also covers a computationally efficient signal modelling method for vertical scanning interferometry and method to improve performance of vertical scanning interferometry with phosphor-based white LED.
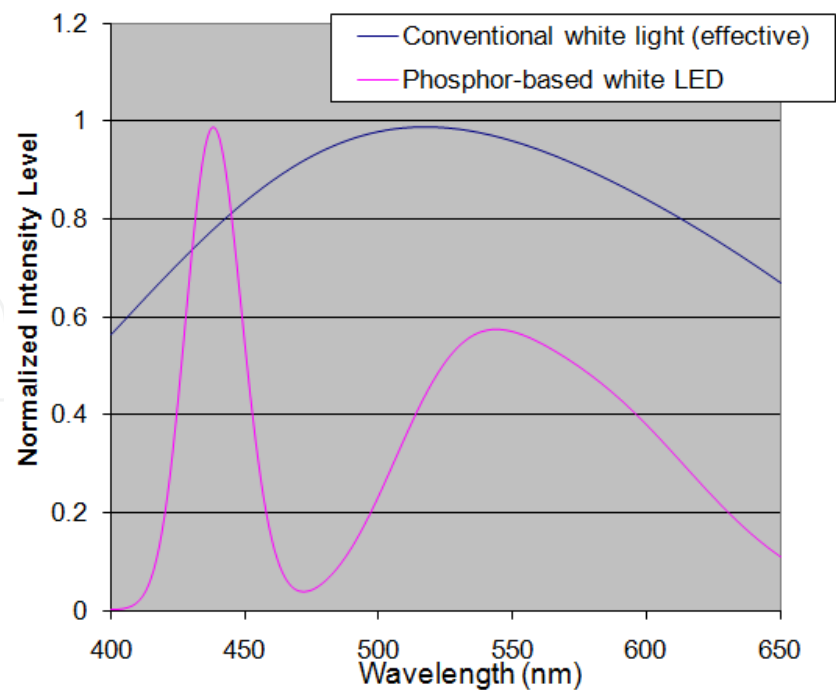
Fig. 5. Comparing effective intensity spectrum of conventional white light and phosphor-based white LED (LXHL-LW6C by LumiLEDs).

2. Theory

Besides optical path difference, the correlogram is affected by the following factors: (1) spectrum of light source (2) numerical aperture of objective (3) optical transfer function of imaging system (4) reflectivity of reference and sample surface (5) phase change at reference and sample surface. The intensity response can be formulated as following:

$$I_{\text{interference}}(z) = C_1 \int_{bandwidth} \int_0^{\theta_0} \{k^2 \times \cos[2k(z-z_0)\cos\theta + \phi]$$

$$\times \sin\theta\cos\theta d\theta\}F(k)dk \qquad (1)$$

where

C_1 is a constant,
z is a independent variable which corresponds to height change by piezoelectric positioner,
z_0 is the height which corresponds to surface profile,
k is angular wave number ($k=2\pi/\lambda$),
$\sin\theta_0$ is numerical aperture (NA) of objective lens,
$\emptyset$ is the phase offset and $F(k)$ is the intensity spectrum of light source.

Detail on derivation and modeling of the intensity response can be found in literature by Chim and Kino (1990), Kino and Chim (1990), de Groot and Lega (2004) and Sheppard and Larkin (1995).

Equation (1) is a generalized model that can simulate the effects of changing spectrum of light source and numerical aperture of objective lens. There is strong correlation between

model parameters and physical setting of the system, for example, the term $F(k)$ in Equation (1) is equal to the intensity spectrum which can be measured by optical spectrum analyzer. The drawback of this generalized model is intensive computational load: as the intensity spectrum of light source is either difficult to be expressed in symbolic form or modelled as Gaussian, Equation (1) has to be solved by numerical integration which is a computationally intensive and time consuming process. Therefore there is a simplified version of the generalized model and it can be expressed as follows:

$$I(z) = I_{dc}(z) + I_{amplitude}(z) \exp\left(\frac{-(z - z_0)^2}{\sigma^2} \right) \cos\left(\frac{2\pi(z - z_0)}{\lambda_m} + \phi \right) \qquad (2)$$

where

z is defocus position (related to optical path difference),
z_0 is related to the profile of sample surface,
I_{dc} is constant value and not related to interference,
$I_{amplitude}$ is amplitude of interference signal,
λ_m is equivalent wavelength of light,
σ is related to coherent length of light and
$\emptyset$ is phase offset.

This simplified model is based on assumptions that the numerical aperture of objective is small and the intensity spectrum of light, $F(k)$ in Equation (1), is single Gaussian function. The advantage of such simplification is computational efficiency, and the drawback is poor correlation between the model parameters and theoretical parameters, for example, the parameter σ in Equation (2) does not have physical meaning (such as the spectrum of light source). As such, the parameters of the simplified model have to be determined empirically, and it is impossible to simulate the correlogram based on specified spectrum and/or numerical aperture value.

To reduce computational load, de Groot and Lega (2004) proposed simplification in frequency domain: Equation (1) is first transformed into frequency domain, followed by simplification, applying numerical integration and lastly inverse Fourier transform back to its original domain. This approach is 200 times faster than direct numerical integration of the generalized model, but it is still a time consuming process due to (1) the use of Fourier and inverse Fourier transform and (2) it still requires numerical integration process.

2.1 Computationally efficient signal modeling

Before looking into the computationally efficient signal modelling, let's look into the cause of intensive computational load of using Equation (1) – numerical integration. Numerical integration is a process calculating the approximated value of a definite integral which can be expressed as following:

$$\int_a^b f(x)dx \approx \frac{(b - a)}{n}\left(\frac{f(a) + f(b)}{2} - \sum_{k=1}^{n-1} f\left(a + k\frac{b - a}{n} \right) \right) \qquad (3)$$

where

n is the number of interval

The accuracy of numerical integration process is proportional to the parameter *n* in Equation (3). However, as *n* goes up, the computational load increases.

There are two cases which numerical integration is required: (1) the integrand may be known for certain region only and/or (2) the anti-derivative of the integrand does not exist. For signal simulation of vertical scanning interferometry, the intensity spectrum, *F(k)* in Equation (1), it is either sampled by spectrum analyzer or modelled as Gaussian (which is not an explicit integral). As such, the generalized model, i.e. Equation (1), has to be solved by numerical integration which is computationally intensive.

Chong et al. (2010a) proposed to remove the numerical integration process by representing a single Gaussian function as a sum of two piecewise cosine functions, which can be expressed as following:

$$a\exp\left(\frac{-(x-x_m)^2}{\sigma^2}\right) = \begin{cases} a_1\cos\left(\frac{2\pi(x-x_m)}{b_1}\right) + a_2\cos\left(\frac{2\pi(x-x_m)}{b_2}\right) & \text{for } (x_m\text{ - }c)\leq x \leq (x_m+c) \\ 0 & \text{else} \end{cases} \quad (4)$$

The transformation from single Gaussian (with parameters of a, x_m and σ) to a sum of two piecewise cosine functions (with parameters of a_1, a_2, b_1, b_2, x_m and c) is modeled as a linear transformation and solved by trust region approach (for generating data) and linear regression, followed by minimizing error of fitting with respect to C_{range}. As a result, the unknown in Equation (4) can now be expressed as following:

$$\begin{cases} a_1 = 0.7888a \\ a_2 = 0.2049a \\ x_m = x_m \\ b_1 = 7.6777\sigma - 0.0078 \\ b_2 = -2.4769\sigma + 0.0024 \\ c = 0.852\min(|b_1|,|b_2|) \end{cases} \quad (5)$$

Next, Equation (1) is derived to elementary form as follows:

$$I_{\text{interference}}(z) = C\int_{bandwidth} k^2 F(k)\int_0^{\theta_0} \cos[2k(z-z_0)\cos\theta + \phi]\sin\theta\cos\theta d\theta dk$$

$$= C\int_{bandwidth} k^2 F(k)\left[-\frac{(2kz\cos\theta - 2kz_0\cos\theta)\sin(2kz\cos\theta - 2kz_0\cos\theta + \phi) + \cos(2kz\cos\theta - 2kz_0\cos\theta + \phi)}{4k^2z^2 - 8k^2z_0z + 4k^2z_0^2}\right]_0^{\theta_0} dk$$

$$= C\int_{k_{ll}}^{k_{ul}} \frac{a\cos\left(2\pi\frac{k-k_m}{b}\right)}{8z_0z - 4z^2 - 4z_0^2}[(2kz\cos\theta_0 - 2kz_0\cos\theta_0)\sin(2kz\cos\theta_0 -$$

$$2kz_0\cos\theta_0 + \phi) + \cos(2kz\cos\theta_0 - 2kz_0\cos\theta_0 + \phi) -$$

$$(2kz - 2kz_0)\sin(2kz - 2kz_0 + \phi) - \cos(2kz - 2kz_0 + \phi)]dk$$

$$= C \int_{k_{ll}}^{k_{ul}} \frac{a \cos\left(2\pi \frac{k-k_m}{b}\right)}{8z_0 z - 4z^2 - 4z_0^2} [2k\cos\theta_0(z-z_0)\sin(2k\cos\theta_0(z-z_0)+\phi) +$$

$$\cos(2k\cos\theta_0(z-z_0)+\phi) - \cos\phi]dk \qquad (6)$$

$$= C\left[\left(g(z,z_0,\theta_0,k_{ul},b) - g(z,z_0,0,k_{ul},b)\right) - \left(g(z,z_0,\theta_0,k_{ll},b) - g(z,z_0,0,k_{ll},b)\right)\right]$$

Let $g(z,z_0,\theta,k,b)$

$$= \frac{D}{4}\left(bU\left(\left(2(\pi-bU)k\cos\left(\frac{(b\phi+2k_m\pi-2\pi k+2bUk)}{b}\right) + b\sin\left(\frac{b\phi+2k_m\pi-2\pi k+2bUk}{b}\right)\right)\bigg/(\pi-bU)^2 + \right.\right.$$

$$\left(-2(\pi+bU)k\cos\left(\frac{b\phi-2k_m\pi+2\pi k+2bUk}{b}\right) + b\sin\left(\frac{b\phi-2k_m\pi+2\pi k+2bUk}{b}\right)\right)\bigg/(\pi+bU)^2\right) +$$

$$\left.\left(b\left(\sin\left(\frac{b\phi+2k_m\pi-2\pi k+2bUk}{b}\right)\bigg/(-\pi+bU) + \sin\left(\frac{b\phi-2k_m\pi+2\pi k+2bUk}{b}\right)\bigg/(\pi+bU)\right)\right)\right)$$

where

$$D = 1\bigg/\left(8zz_0 - 4z^2 - 4z_0^2\right)$$

$$U = (z-z_0)\cos\theta$$

Chong et al.'s model (2010a) reduces the computational time by 256800 times compared to conventional direct numerical integration on Equation (1), and it is 2784 times faster than de Groot and Lega (2004) 's approach.

2.2 Phosphor-based white LED

Phosphor-based white LED consists of single color LED (normally blue) and phosphor of different color (normally yellow) to produce white light, so there are two peaks in its spectrum and the intensity spectrum can be expressed as follows:

$$f(k) = BYratio \times e^{-\left(\frac{k-k_{blue}}{\sigma_{blue}}\right)^2} + e^{-\left(\frac{k-k_{yellow}}{\sigma_{yellow}}\right)^2} \qquad (7)$$

where

k is angular wave number ($=2\pi/\lambda$)
k_{blue} and k_{yellow} indicate the peak angular wave number of blue and yellow light
σ_{blue} and σ_{yellow} indicate the spread of blue and yellow light in spectrum domain

In general, the angular wave number of blue and yellow light are 14.37 rad/nm (438nm) and 11.25 rad/nm (558nm) respectively, the spread of blue and yellow light in spectrum domain are 0.4941 rad/nm and 1.439 rad/nm; these values vary slightly across manufacturers/model.

Compared to conventional white light (with reference to Fig. 5), the intensity spectrum of phosphor-based white LED is significantly different.

3. Effects of phosphor-based white LED on vertical scanning interferometry

As mentioned earlier, the intensity spectrum of phosphor-based white LED is significantly different from conventional lighting which most prior arts adopted. In this section, the effects of phosphor-based white LED on vertical scanning interferometry in correlogram and reconstructed surface profile level are investigated by simulation, followed by experimental verification.
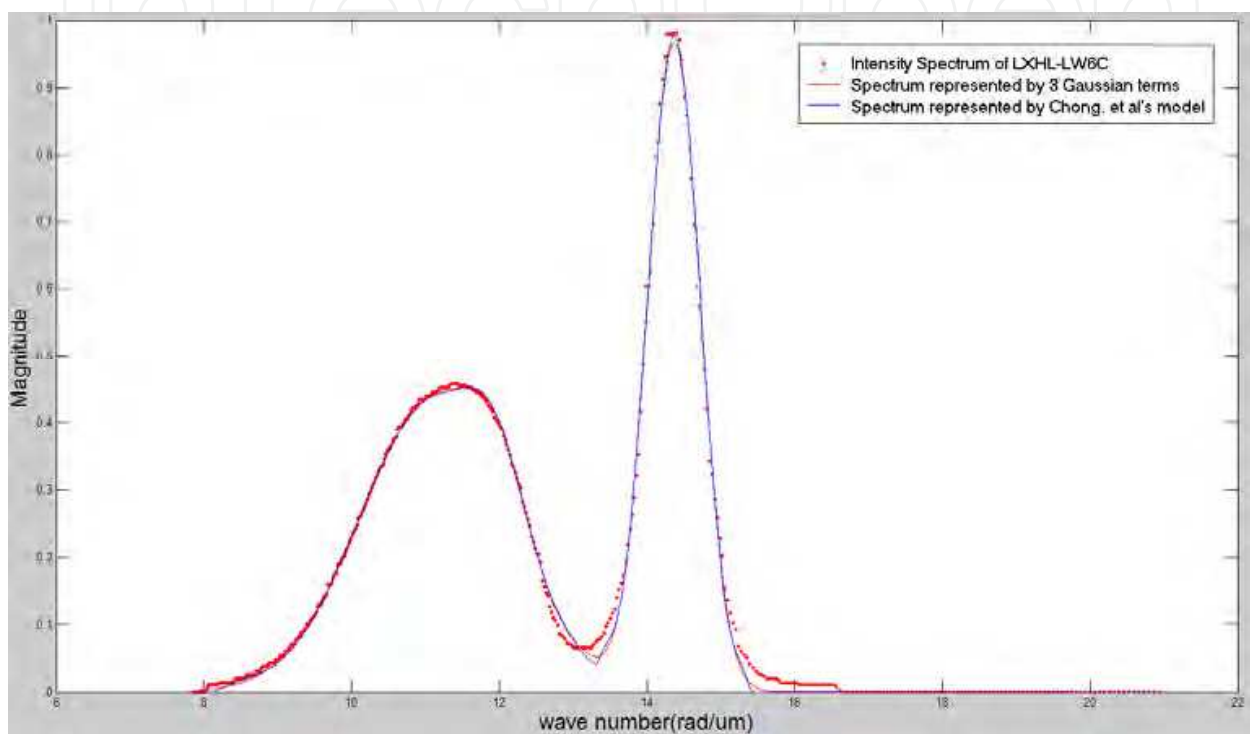

Fig. 6. Intensity spectrum of phosphor-based LED, LXHL-LW6C by LumiLEDs and comparison between its presentations by three Gaussian functions and Chong et al.'s method.

To study the effects of phosphor-based white LED, a commercial off the shelf phosphor-based white LED, LXHL-LW6C by LumiLEDs is selected, and the numerical aperture of objective is assumed to 0.4 which is a typical value for 20x objectives. This configuration is adopted for both simulation and experimental verification.

To simulate the correlogram of LXHL-LW6C by LumiLED, the intensity spectrum (as shown in Fig. 6) is first fitted to three Gaussian functions by non-linear least square fitting method; next each Gaussian terms is replaced with a sum of two piecewise cosine functions according Equation (4) and Equation (5); by Equation (6), contribution of each cosine term is calculated; lastly, the resultant intensity response is the sum of contribution by six cosine terms.

Fig. 6 shows that Chong et al.'s method represents the intensity spectrum of LXHL-LW6C by LumiLED well compared to representation by three Gaussian functions and the original intensity spectrum.

3.1 Effects on correlogram

Based on the intensity spectrum of LxHL-LW6C and numerical aperture of 0.4, the corresponding correlogram is simulated using the computational efficient signal modelling by Chong et al and shown in Fig. 7 (b). The distinctive feature highlighted in Fig. 7 (b) is the result of having two peaks in the spectrum of phosphor-based white LED.
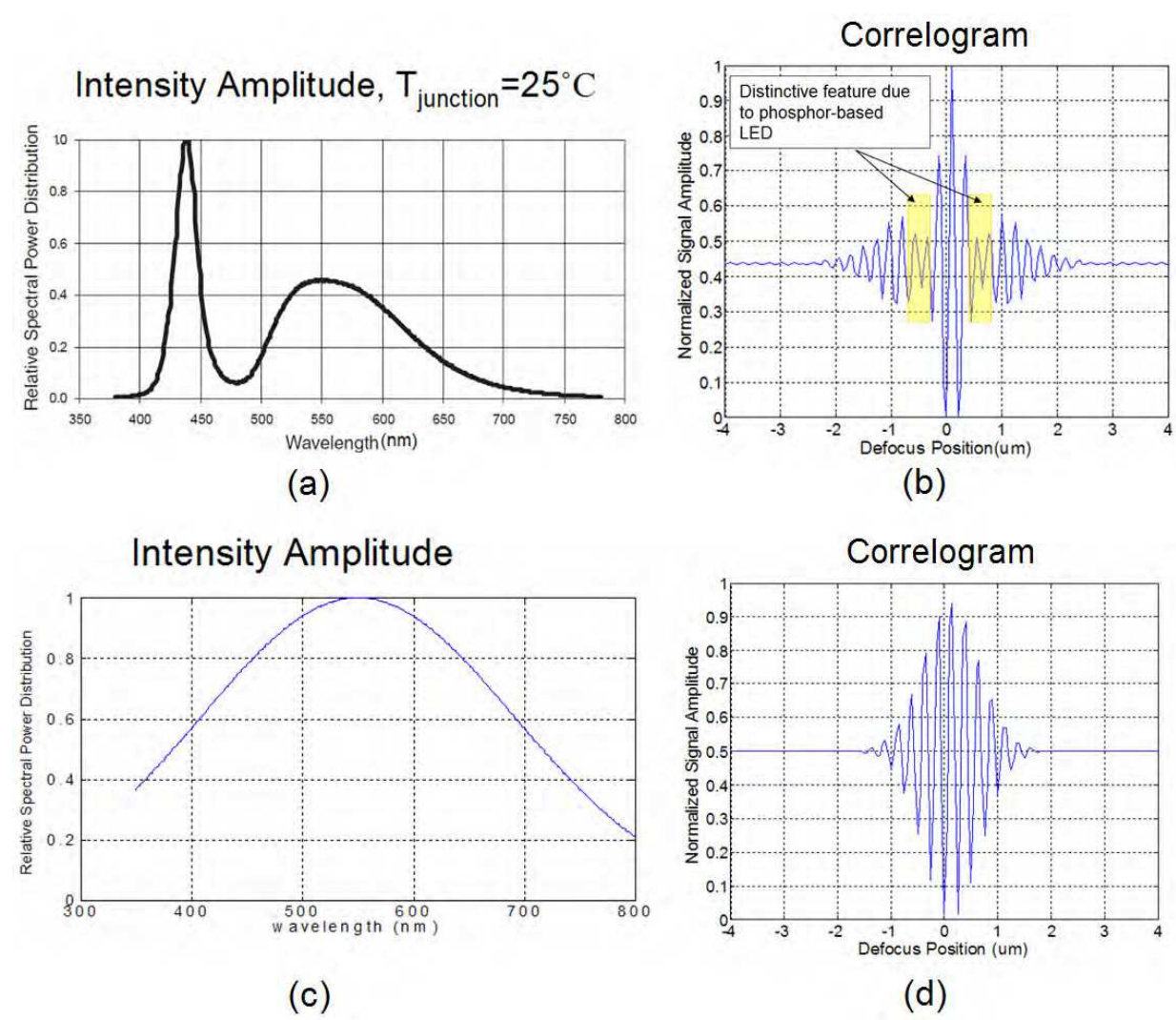

Fig. 7. Comparing spectrum and correlogram of phosphor-based white LED and conventional white light: (a) spectrum of phosphor-based LED, LXHL-LW6C; (b) simulated correlogram based on spectrum of (a); (c) effective spectrum of conventional white light; (d) simulated correlogram based on spectrum of (c).

As shown in Fig. 7, the correlogram of vertical scanning interferometry using phosphor-based white LED is significantly different from that using light source of Gaussian spectrum (as shown in Fig. 7(c) and (d)).

Next, an experimental verification is conducted to verify the simulation result. The experiment configuration is as follows: a 40x Nikon mirau-based interferometric objective with numerical aperture of 0.4 and phosphor-based white LED from LumiLEDs LXHL-LW6C was used.
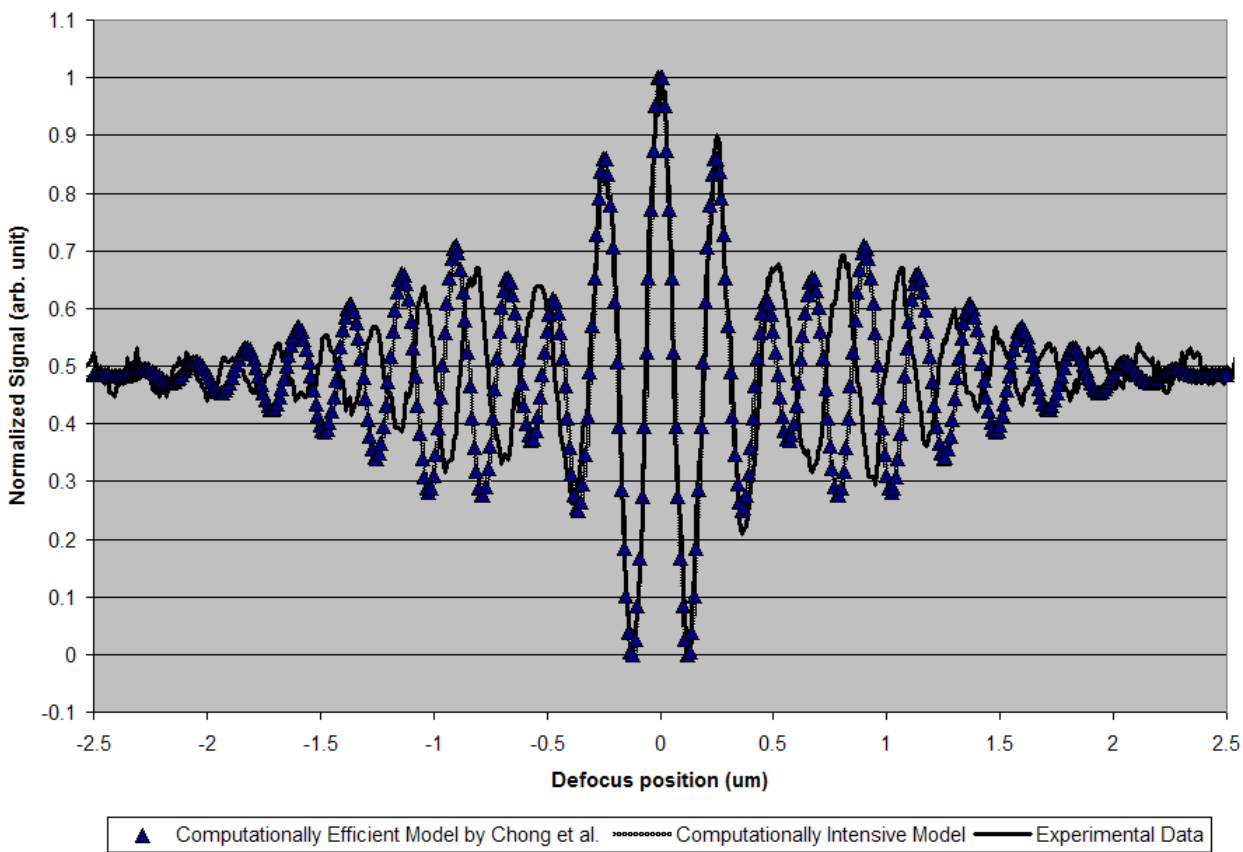
Fig. 8. Graphical comparison between computationally efficient signal modeling by Chong et al., computationally intensive model and experimental data.

Fig. 8 graphically compares the experimental data with simulation data, it shows that the distinctive feature due to the use of phosphor-based white LED (highlighted in Fig. 7(b)) is consistent with the experimental data.

By experiment and simulation, it is shown that the intensity response (also known as correlogram) of vertical scanning interferometry using phosphor-based white LED significantly different from light source of Gaussian spectrum. The fringe contrast function (envelope function of correlogram) is not longer a single Gaussian function (Chong, Li, & Wijesoma, 2010b).

3.2 Effects of reconstructed height profile

As correlogram alone does not provide information on height, a reconstruction algorithm is required to transform correlogram into height information. There are two categories for surface height profile reconstruction algorithm: (1) fringe contrast based approach and (2) phase-based approach. Fringe contrast based approach finds the maximum of fringe contrast function which corresponds to the height profile; while phase-based approach transforms intensity response into frequency domain, followed by phase signal analysis.

This section investigates the effects of phosphor-based LED on three reconstruction algorithms proposed by Gaussian fitting method (Mingzhou et al., 2005), Centroid approach (Ai & Novak, n.d.), and Frequency domain analysis (FDA) (P. J. de Groot & Deck, 1994)

respectively. Among these three algorithms, only FDA is phase-based approach; the other two are fringe contrast based approach. Among these two methods, the major difference is that Gaussian fitting method by Mingzhou et al assumes the fringe contrast function is a Gaussian signal while the centroid approach does not.

Mingzhou et al.'s method recovers height by first finding the envelope of the correlogram, followed by Gaussian fitting. Ai and Novak proposed that the centroid of the correlogram corresponds to the maximum of fringe. As phase-based approach, Groot and Deck's method breaks down the white light into multiple single wavelength components and applies phase signal analysis similar to phase shifting interferometry.

Simulation is used for investigating the effects of phosphor based white LED on reconstructed height profile. For comparison purpose, two sets of data are simulated: one is based on light with Gaussian spectrum; another one is based on phosphor-based white LED, LXHL-LW6C by LumiLEDs. A line profile of 1um step height is selected, the line profile consists of 256 surface points and each surface point has a corresponding intensity response. The sampling interval of the intensity response is 50nm, and each intensity response is corrupted by Gaussian white noise (zero mean, variance of 0.05). Next we reconstructed these two sets of data using these three construction algorithms mentioned earlier, and the reconstructed profiles are shown in Fig. 9 and Fig. 10. The repeatability (in term of standard deviation) and accuracy of reconstructed profiles are further analyzed.
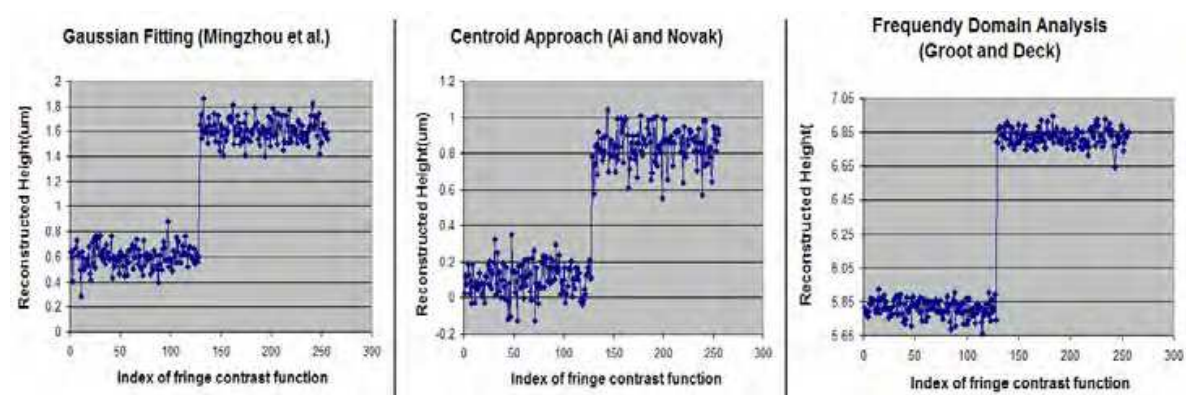

Fig. 9. For phosphor-based LED set, 1um step height reconstructed using (a) Gaussian Fitting by Mingzhou et al. (b) Centroid approach by Ai and Novak (c) Frequency domain analysis by Groot and Deck
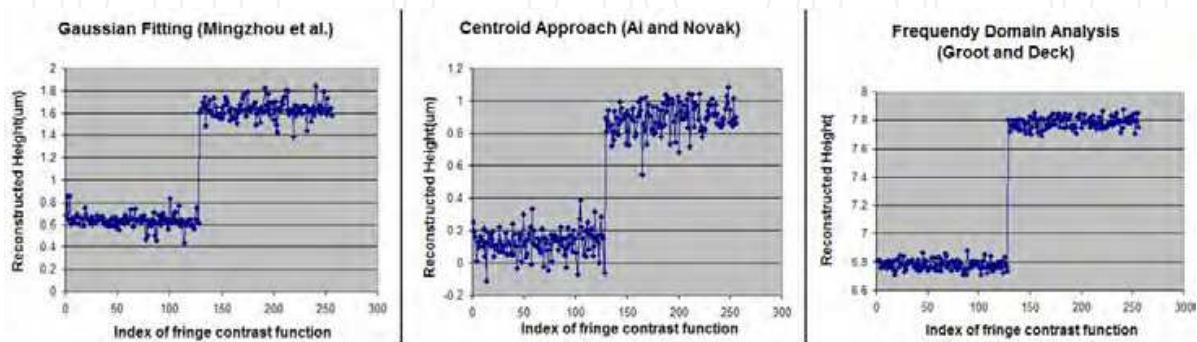

Fig. 10. For light source of Gaussian spectrum, 1um step height reconstructed using (a) Gaussian Fitting by Mingzhou et al. (b) Centroid approach by Ai and Novak (c) Frequency domain analysis by Groot and Deck
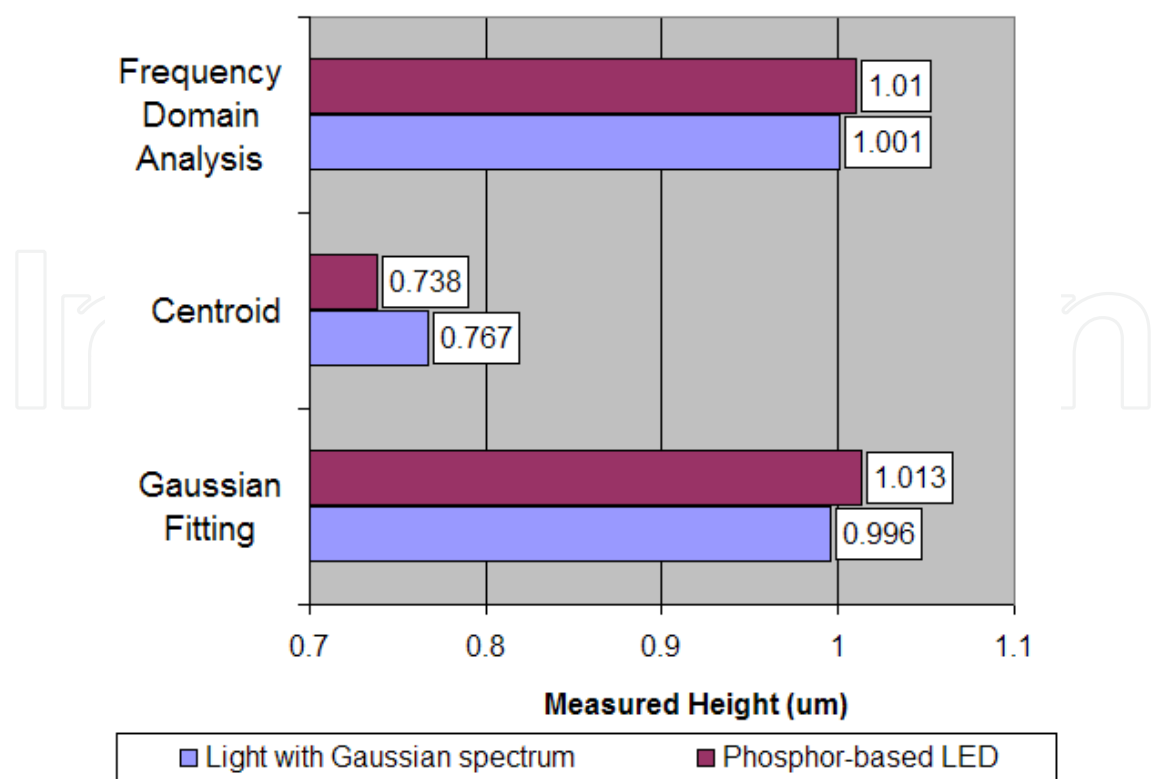
Fig. 11. Comparing measurement accuracy of different algorithms between different light sources, ideal value is 1um.

Fig. 11 shows the comparison of accuracy among different algorithms using different lighting. As the accuracy of individual algorithm is highly dependent on the complexity of the algorithm, it is beyond the scope of this investigation. However it is noticeable that the accuracy of all three algorithms decreases as the light is switched to phosphor-based white LED.

Fig. 12 shows the comparison of measurement repeatability among different algorithms using different lighting, and it is clear that the use phosphor-based LED decreases the repeatability of measurement (standard deviation is inversely proportional to repeatability) at different scale: Gaussian fitting method by Mingzhou et al. suffers most, followed by frequency domain analysis by Groot and Deck, lastly the centroid approach by Ai and Novak. This observation can be explained as follows:

- For the centroid approach by Ai and Novak: This method does not make assumption on the fringe contrast function, so the change in fringe contrast function has relatively little effect on its reconstruction.
- For Gaussian fitting by Mingzhou et al.: This method assumes that the fringe contrast function is a Gaussian function, so it suffers the worst repeatability. As the assumption on the fringe contrast function is not valid, the fitting process is unable to produce good result.
- For the frequency domain analysis by Groot and Deck: Although this method processes the correlogram in the frequency domain only, the change in fringe contrast function does affect the amount and the quality of information selected for frequency domain analysis. This effect leads to improvement discussed in next session.
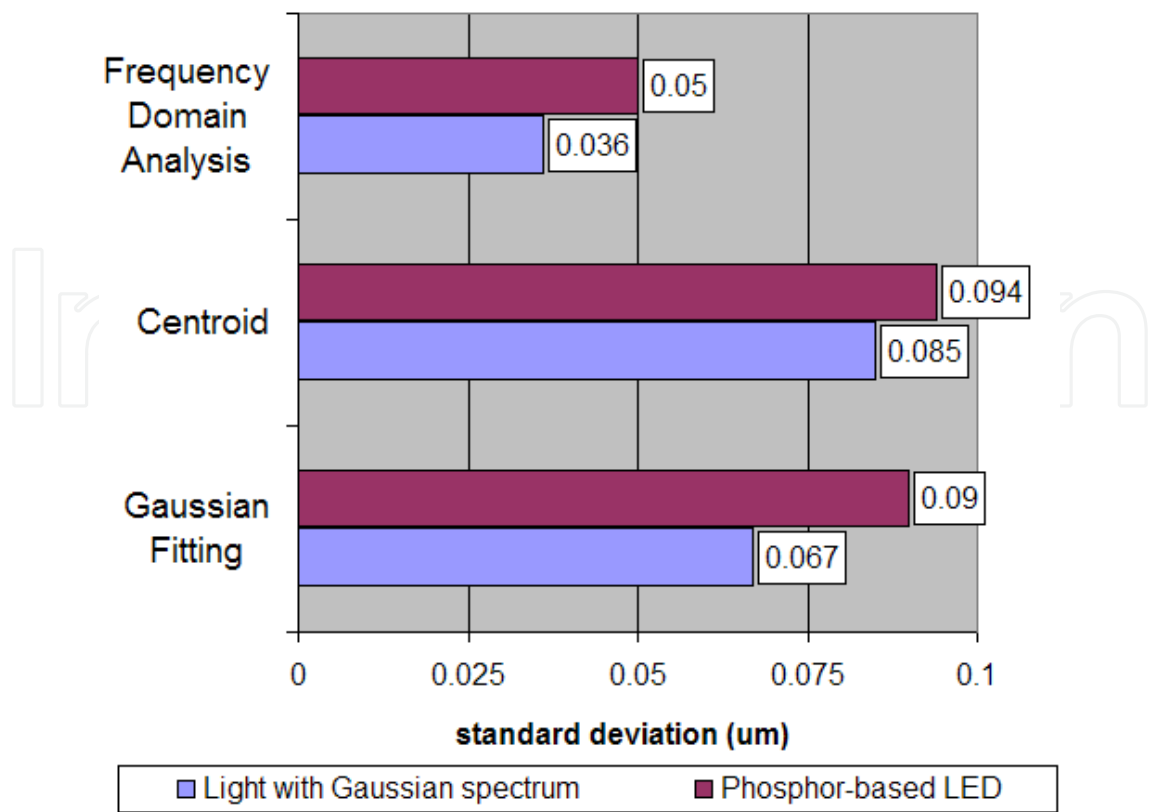
Fig. 12. Comparing the measurement repeatability of different algorithms between different light sources: measurement repeatability is inversely proportional to the standard deviation of perfectly flat surface, ideal value is zero.

4. Modification and improvement for phosphor-based white LED on VSI

As identified earlier, phosphor-based white LED degrades the performance of two reconstruction algorithms (Gaussian fitting method and Frequency domain analysis approach) as it breaks the assumption adopted by these reconstruction algorithms. These undesired effects of phosphor-based white LED can be avoided by either redesigning reconstruction algorithm that does not assume the distribution of intensity spectrum or setting constraint on the input to existing reconstruction algorithm such that the assumption is valid. Redesigning a reconstruction algorithm is beyond the scope of this chapter, so a constraint is applied to make assumption required by Gaussian fitting and frequency domain analysis approach valid.

For Gaussian fitting method, the two valleys (distinctive features highlighted in Fig. 7 (b)) make the fringe contrast function has 3 peaks and can not be modelled as single Gaussian function. However as shown in Fig. 13, the envelope of correlogram between two valleys (distinctive features highlighted in Fig. 7 (b)) can be reasonably modelled as single Gaussian, setting a constraint selecting only these data for single Gaussian fitting would fulfil the assumption of the original Gaussian fitting approach. So, instead of fitting the whole correlogram to a Gaussian, Gaussian fitting approach is modified such that it fit subset of correlogram to a Gaussian.

For frequency domain analysis approach, the required assumption is that there should be only one peak in the spatial frequency ranges from 20rad/um to 30 rad/um which

correspond to wavelength of 628nm and 419nm. However for phosphor-based white LED, there are two peaks in the frequency ranges of interest (as shown in Fig. 14(a)), so we applied a constraint on the input for frequency domain analysis such that it would not have two peaks in spatial frequency domain analysis. As the distinctive features are the result of phosphor-based LED, we applied only data between these two features for frequency domain analysis. Fig. 14 (b) confirms that the assumption of frequency domain analysis is met by reducing the amount of data for frequency domain analysis, there is only one distinct peak in spatial frequency domain.
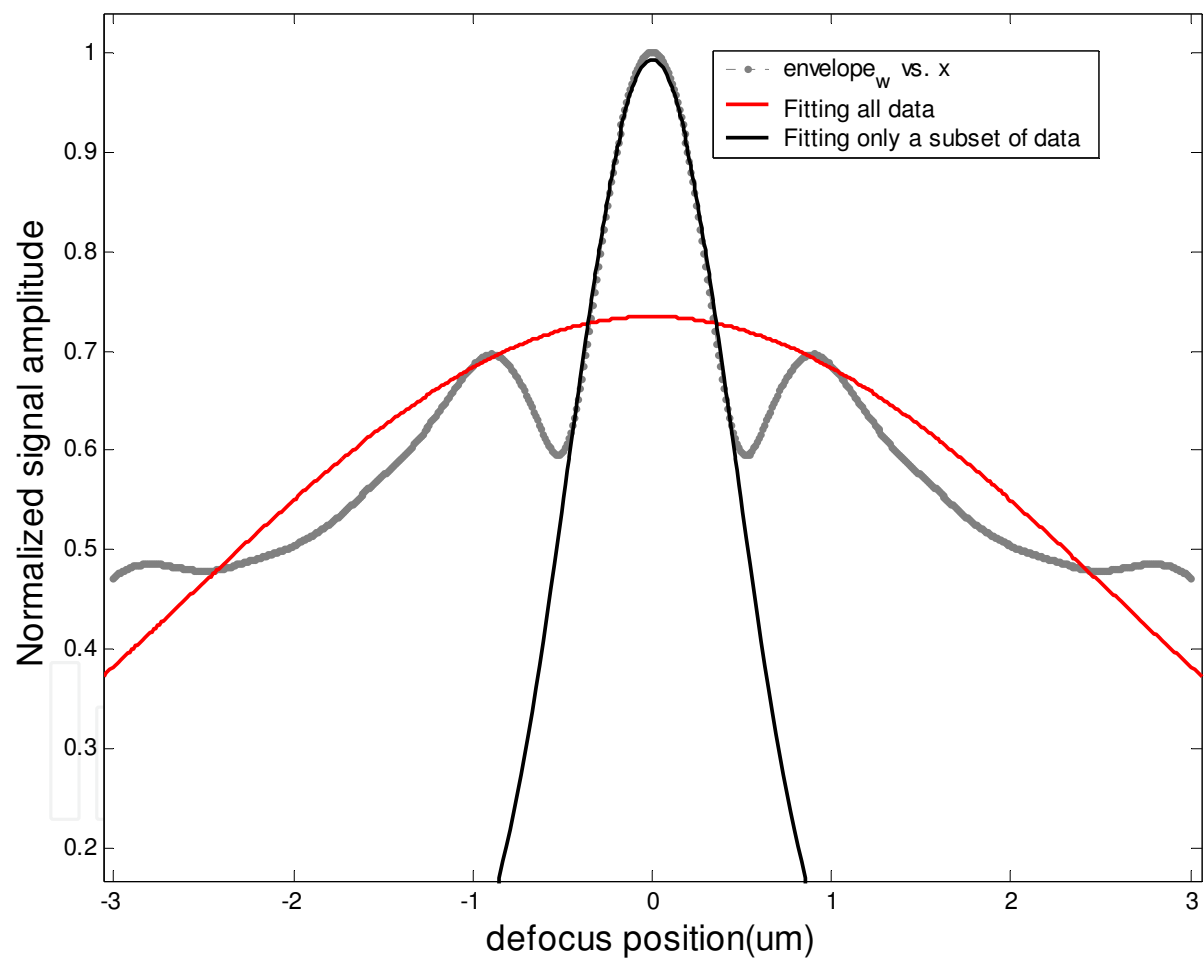
Fig. 13. Fitting the fringe contrast function with single Gaussian: Selecting a subset of data (such as -0.5um<=defocus position<= 0.5um) would lead to a good fit compared to selecting all data.
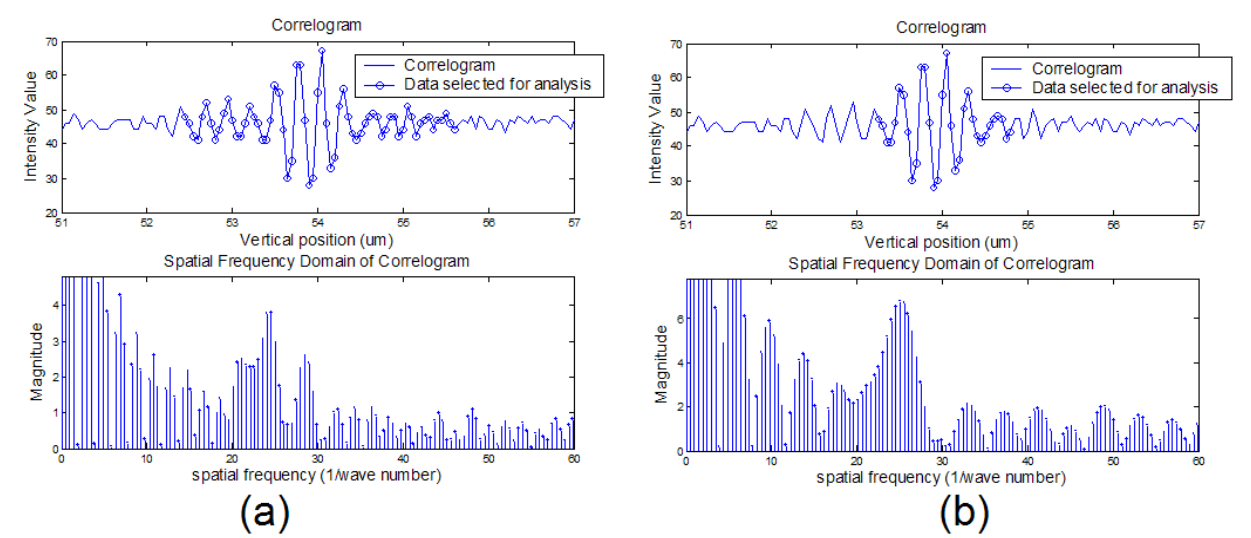
Fig. 14. Illustrating the effects of selecting (a) 64 data (b) 32 data around the maximum of correlogram in spatial frequency domain. According to FDA approach, there should be only 1 peak (in the region around 20 to 30 rad/um), this assumption is met in (b) which 32 data around peak are selected.

Fig. 15 shows that the proposed modification on Gaussian fitting approach and frequency domain analysis works, the constraint on the input to reconstruction algorithms improves the measurement repeatability.
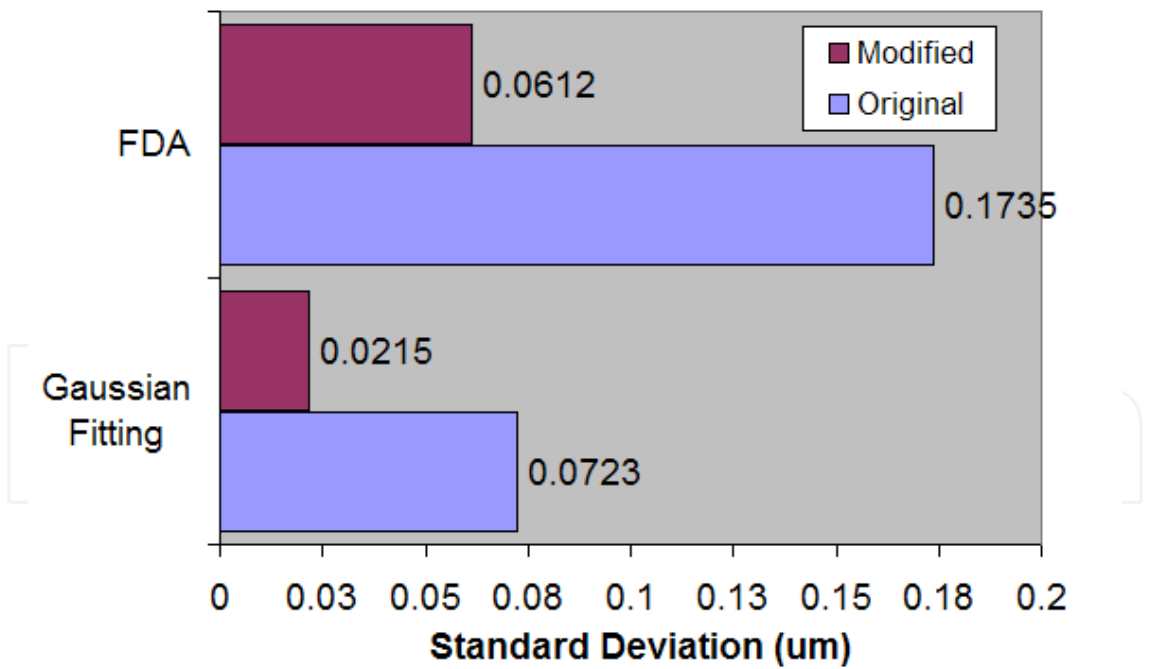

Fig. 15. Simulation verification on the proposed modification: Comparing standard deviation of measuring perfectly flat surface reproduced by proposed modification and original.

As an experimental verification, the configuration is identical to the earlier simulation but measured a 10um±80nm standard step height. 256 correlograms are collected at sampling

interval of 50nm, the repeatability of measuring optically flat surface was used to measure the performance of modified Gaussian fitting, modified frequency domain analysis, original Gaussian fitting and original frequency domain analysis.
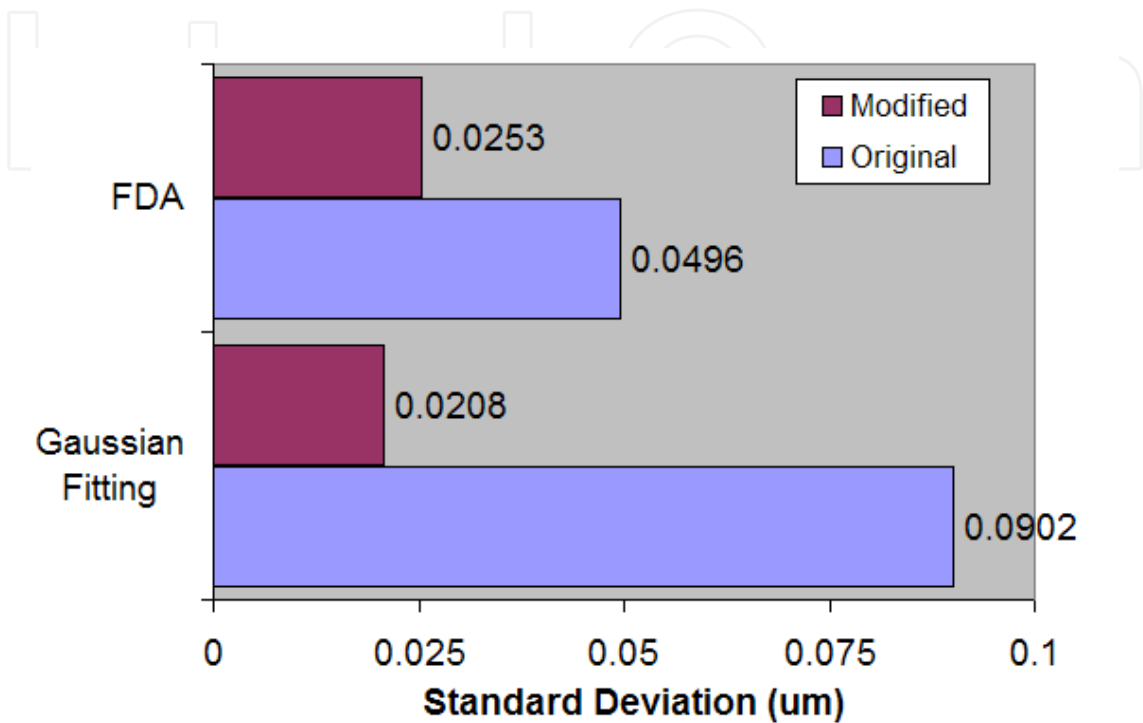

Fig. 16. Experimental verification on the proposed modification: Comparing standard deviation of measuring perfectly flat surface reproduced by proposed modification and original.

Fig. 16 shows that the repeatability of both modified reconstruction algorithm are better than original one, the result agrees with simulation result, but it is controversial to common norm that more data leads to better result.

The result shows that for surface reconstruction of vertical scanning interferometry, it is more important to fulfil the assumption of reconstruction algorithm rather than fitting as many data as possible. The modification of inputting a subset of correlogram (which is around the maximum) improves the performance of reconstruction algorithm for phosphor-based LED, and it is applicable to reconstruction algorithm of both fringe contrast based and phase-based approach.

5. Conclusion

In this chapter, it is shown that the use of phosphor-based LED on vertical scanning interferometry affect the repeatability and accuracy of vertical scanning interferometry, especially repeatability. The effect on the correlogram is inevitable, as the fringe contrast function can not longer be modelled as single Gaussian function. The effect on the

reconstructed height profile varies depending on the assumption adopted by individual reconstruction algorithm. However the undesired effects of phosphor-based white LED can be removed by applying a constraint on the input to existing reconstruction algorithm.

6. Acknowledgment

7. References

Ai, C., & Novak, E. K. (n.d.). Centroid approach for estimating modulation peak in broad-bandwidth interferometry. *United States Patent*. Retrieved from http://www.freepatentsonline.com/5633715.html

Chim, S. S. C., & Kino, G. S. (1990). Correlation microscope. *Optics Letters*, *15*(10), 579-581. doi:10.1364/OL.15.000579

Chong, W. K., Li, X., & Wijesoma, S. (2010a). Computationally efficient signal modeling for vertical scanning interferometry. *Applied Optics*, *49*(26), 4990-4994. doi:10.1364/AO.49.004990

Chong, W. K., Li, X., & Wijesoma, S. (2010b). Effects of phosphor-based LEDs on vertical scanning interferometry. *Optics Letters*, *35*(17), 2946-2948. doi:10.1364/OL.35.002946

de Groot, P., & Colonna de Lega, X. (2004). Signal Modeling for Low-Coherence Height-Scanning Interference Microscopy. *Applied Optics*, *43*(25), 4821-4830. doi:10.1364/AO.43.004821

Groot, P. J. de, & Deck, L. L. (1994). Surface profiling by frequency-domain analysis of white light interferograms. In C. Gorecki & R. W. T. Preater (Eds.), *Optical Measurements and Sensors for the Process Industries* (Vol. 2248, pp. 101-104). SPIE. Retrieved from http://dx.doi.org/10.1117/12.194308

Guo, H., Zhao, Z., & Chen, M. (2007). Efficient iterative algorithm for phase-shifting interferometry. *Optics and Lasers in Engineering*, *45*(2), 281-292. doi:10.1016/j.optlaseng.2005.11.002

Gurov, I., Ermolaeva, E., & Zakharov, A. (2004). Analysis of low-coherence interference fringes by the Kalman filtering method. *Journal of the Optical Society of America A*, *21*(2), 242-251. doi:10.1364/JOSAA.21.000242

Kino, Gordon S., & Chim, S. S. C. (1990). Mirau correlation microscope. *Applied Optics*, *29*(26), 3775-3783. doi:10.1364/AO.29.003775

Mingzhou, L., Chenggen, Q., Cho Jui, T., Ivan, R., & Shihua, W. (2005). Measurement of transparent coating thickness by the use of white light interferometry. *Third*

International Conference on Experimental Mechanics and Third Conference of the Asian Committee on Experimental Mechanics (Vol. 5852, pp. 401-406). SPIE.

Pavliček, P., & Soubusta, J. (2004). Measurement of the Influence of Dispersion on White-Light Interferometry. *Applied Optics*, *43*(4), 766-770. doi:10.1364/AO.43.000766

Sheppard, C. J. R., & Larkin, K. G. (1995). Effect of numerical aperture on interference fringe spacing. *Applied Optics*, *34*(22), 4731-4734. doi:10.1364/AO.34.004731
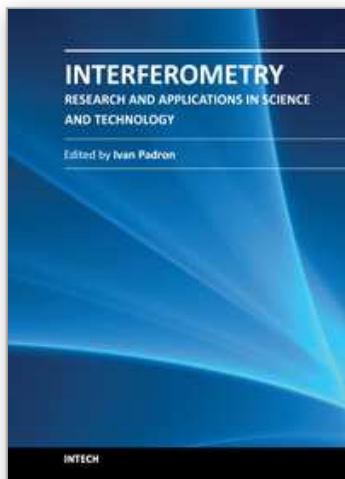
Interferometry - Research and Applications in Science and Technology
Edited by Dr Ivan Padron

ISBN 978-953-51-0403-2
Hard cover, 462 pages
Publisher InTech
Published online 21, March, 2012
Published in print edition March, 2012

This book provides the most recent studies on interferometry and its applications in science and technology. It is an outline of theoretical and experimental aspects of interferometry and their applications. The book is divided in two sections. The first one is an overview of different interferometry techniques and their general applications, while the second section is devoted to more specific interferometry applications comprising from interferometry for magnetic fusion plasmas to interferometry in wireless networks. The book is an excellent reference of current interferometry applications in science and technology. It offers the opportunity to increase our knowledge about interferometry and encourage researchers in development of new applications.

INTECH
open science | open minds